JACS
JOURNAL OF THE AMERICAN CHEMICAL SOCIETY
pubs.acs.org/JACS
Article

3D Unconventional Superconductivity in Bulk LaO

Zhifan Wang,[#] Jingkai Bi,[#] Jiayuan Zhang,[#] Wenmin Li, Yuxuan Liu, Dao-Xin Yao,[*] Zheng Deng,[*] Changqing Jin, Yifeng Han,[*] and Man-Rong Li[*]

Cite This: J. Am. Chem. Soc. 2026, 148, 13309−13316

Read Online

ACCESS | Metrics & More | Article Recommendations | Supporting Information

ABSTRACT: Lanthanum-based compounds are cornerstones of superconductivity research, yet the La 5d orbitals typically remain empty spectator states far above the Fermi level (E_F). While superconductivity has been induced in LaO up to 5.37 K in tensile epitaxy films, the intrinsic ground state of the bulk phase has remained controversial mostly due to synthetic challenges, with early reports suggesting a metallic nature. Here we report the high-pressure and high-temperature synthesis of pure bulk rock-salt LaO and unveil its intrinsic type-II superconductivity with a transition temperature (T_C) of ∼6 K at ambient pressure. The bulk T_C is further enhanced to 6.9 K in $La_{1-x}Y_xO$ at x = 0.10, where Y doping leads to lattice contraction (chemical pressing) and a remarkable increase in electron carrier concentration. Strikingly, applying physical pressure further enhances the T_C to a maximum of 12.7 K at 20 GPa, the highest T_C in lanthanum monochalcogenides LaX (X = S, Se, Te, and O) to date. This pressure dependence is diametrically opposed to the behavior observed in films, and occurs despite a pressure-induced reduction in the density of states at E_F—a trend that sharply contradicts the conventional phonon-mediated BCS mechanism. Our first-principles calculations reveal that compressive strain modifies the crystal field splitting to enhance La 5d/O 2p hybridization, fostering a three-dimensional multipocket Fermi surface favorable for spin/orbital fluctuation-mediated pairing. This work clarifies the intrinsic superconductivity of bulk LaO and provides a foundation for designing new rare-earth-based superconductors with higher T_C.

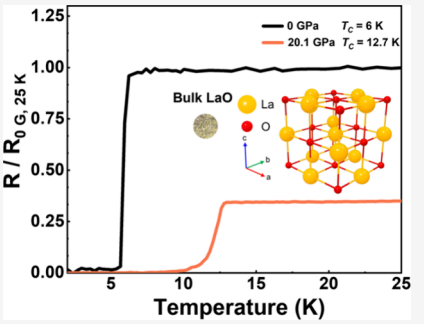

1. INTRODUCTION

Lanthanum-based compounds constitute one of the most fertile grounds for discovering high-temperature superconductivity, exemplified by the pioneering cuprates,[1,2] the recently discovered nickelates,[3−5] and iron-based superconductors.[6] In the vast majority of these systems, however, the lanthanum ion adopts a stable trivalent state (La^{3+}).[7] In this configuration, the 5d and 5s orbitals remain empty and energetically remote from the E_F, relegating La to the role of a passive structural spacer or charge reservoir. A rare and intriguing departure from this paradigm is found in the lanthanum monochalcogenides LaX (X = S, Se, Te, O), where lanthanum adopts a divalent state (La^{2+}).[8−10] Here, the typically dormant 5d electrons become active, directly populating the conduction bands, and offering a unique frontier to explore unconventional quantum phases driven by 5d-orbital physics.

Among this family,[11,15] lanthanum monoxide (LaO) stands out as a particularly enigmatic candidate. While thermodynamic considerations suggest it should crystallize in a simple rock-salt structure, its synthesis requires stringent high-pressure and high-temperature (HPHT) conditions. Early studies on bulk LaO two decades ago reported a metallic ground state, leaving the question of its superconductivity dormant. Interest was reignited recently when superconductivity up to 5.37 K was observed in epitaxial LaO thin films.[12−16] However, interpretation of these film results is complicated by substrate-induced tetragonal distortions, where tensile strain was seemingly required to stabilize the superconducting phase. This has led to a dichotomy in the field: Is superconductivity intrinsic to the ideal rock-salt LaO lattice, or is it an artifact of interfacial strain? Furthermore, while initial theoretical works proposed a conventional phonon-mediated mechanism,[15−17] they struggled to reconcile the relationship between lattice volume (V) and superconducting temperature (T_C) across different experimental regimes.

Resolving these fundamental questions requires accessing the pristine bulk phase, free from substrate clamping. Unlike thin films, where lattice parameters are pinned, bulk LaO allows for the continuous tuning of the lattice via hydrostatic pressure and chemical doping, providing a clean testbed for the pairing mechanism. Specifically, clarifying how T_C responds to isotropic compression is critical; for a conventional phonon-mediated superconductor, pressure-induced broadening of bands typically suppresses the density of states (DOS) and T_C.[17] Conversely, an enhancement of T_C under pressure-analogous to the behavior seen in cuprates and iron-based systems[18,19] would signal the presence of alternative pairing

Received: January 8, 2026
Revised: February 19, 2026
Accepted: March 6, 2026
Published: March 18, 2026

https://doi.org/10.1021/jacs.6c00519
J. Am. Chem. Soc. 2026, 148, 13309−13316

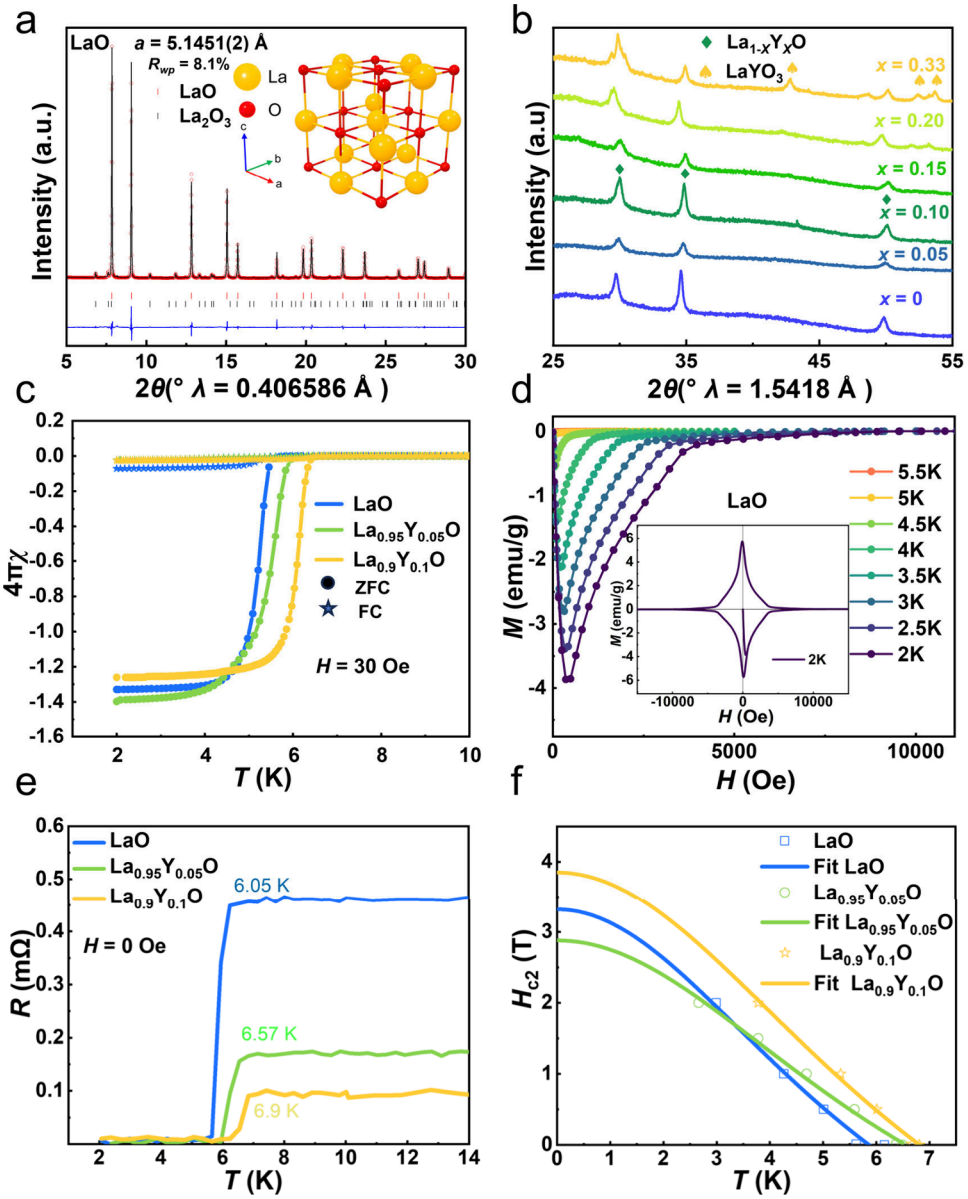

Figure 1. (a) Rietveld refinements of the SPXD data for LaO. The red circle represents the calculated data, the black line the observed fit, and the deep blue line the difference. The upper red and lower black ticks marks the positions of Bragg reflections of LaO ($Fm\bar{3}m$, 97.29%) and La_2O_3 ($P\bar{3}m1$, 2.71%), The inset shows the crystal structure of LaO. (b) XRD patterns of $La_{1-x}Y_xO$ (x = 0, 0.05, 0.10, 0.15, 0.20, 0.33). (c) Temperature dependence of the superconducting fraction for $La_{1-x}Y_xO$ (x = 0, 0.05, and 0.10,). (d) H curves of LaO measured below T_C in the field range of 0−1 T, with the inset displaying the $M(H)$ curves at 2 K over an extended field range of −1 to 1 T. (e) Temperature dependence of resistance for $La_{1-x}Y_xO$ (x = 0, 0.10, 0.15) at ambient pressure. (f) Temperature dependences of H_{c2} of Y = 0, 0.05, and 0.10.

interactions. Lavroff et al. showed in LaB_6 that the localization of Fermi-level states is crucial for electron−phonon coupling (EPC): La 4*f*-B π hybridization suppresses EPC, yielding T_C = 0.45 K.[20] Zhai et al. found in transition-metal diborides that anisotropic strain selectively tunes metal−boron hybridization and bond covalency, thereby modulating phonon-mediated superconductivity.[21] These studies offer a useful framework for understanding how orbital hybridization and state localization control superconductivity. In this study, we revisit the bulk limit of LaO. By mastering the HPHT synthesis of stoichiometric samples, we not only confirm its intrinsic type-II superconductivity but also unveil a pressure-tunable phase diagram that defies conventional BCS expectations.

2. EXPERIMENTAL AND METHODS

HPHT Synthesis and Phase Stability

La_2O_3 (99.999%, Macklin) and Y_2O_3 (99.999%, Macklin) powders were annealed at 1273 K in air before transferred into an argon-filled glovebox. La metal (99.7% (metal), mesh 40, Alfa Aesar) was received packed under Ar and opened in a glovebox. The phase analysis of La metal was performed by X-ray diffraction (XRD) in a sealed holder. La was confirmed to be the hexagonal $P6_3/mmc$ phase. $La_{1-x}Y_xO$ (x = 0, 0.05, 0.10) were synthesized by HPHT method in our 420-type six-sided top press.[22] The raw materials La_2O_3, La and Y_2O_3 with certain stoichiometric ratios were fully mixed in an agate mortar in Ar-filled glovebox. Slightly excessive (~3% by weight/mol) La was applied to account for the possible surface oxidation of La metal. Afterward, the mixture was pressed into blocks with a diameter and height of 0.55 and 0.70 cm, respectively, under 5 MPa in a glovebox. Subsequently,

https://doi.org/10.1021/jacs.6c00519
J. Am. Chem. Soc. 2026, 148, 13309−13316

the block was assembled into a synthetic block and placed in a six-sided top press. For all HPHT experiments, the pressure was increased to 5 GPa and then the assembly was heated at 1573 K for 2−4 h before quenching to room temperature. The pressure was then slowly decompressed to ambient. The recovered capsules were opened, and the $La_{1-x}Y_xO$ (x = 0, 0.05, 0.10) sample pellets were cleaned minimally by breaking or scraping off remaining large pieces of the capsule to remove residue and minimize impurity. Samples were then stored in an Ar-atmosphere glovebox.

The synthesized bulk polycrystalline $La_{1-x}Y_xO$ exhibited golden-yellow color with metallic luster. The phase purity was characterized by powder XRD and synchrotron powder X-ray diffraction (SPXD). It is noteworthy that the polycrystalline $La_{1-x}Y_xO$ undergoes gradual degradation when exposed to air. Comparative XRD analyses under different storage conditions revealed that samples stored in Ar atmosphere maintained unchanged, whereas those exposed to air developed prominent $La(OH)_3$ peaks in XRD patterns. Consequently, all samples were stored in our Ar-filled glovebox to preserve their structural integrity.

Phase and Structural Analyses

XRD patterns were obtained using a powder X-ray diffractometer (MiniFlex 600, Rigaku, Japan) equipped with Cu Kα tube (40 kV and 15 mA). The surfaces of the as-made sample pellets were polished smooth and mounted with nonpeak modeling clay for XRD data collection to assess phase purity. SPXD data were acquired at the beamline BL14B (λ = 0.6886 Å) of the Shanghai Synchrotron Radiation Facility (SSRF) and beamline BL44B2 (λ = 0.406586 Å) of SPring-8, Japan. Rietveld refinements of the SPXD data were performed using Topas-Academic *V6* software.[23]

Magnetic and Electrotransport Measurements

Magnetic properties were measured using a Physical Property Measurement System (PPMS-9 T, Quantum Design). The temperature-dependent zero-field cooling (ZFC) and field cooling (FC) magnetic susceptibility data were collected in 2−300 K under an applied magnetic field of 0.003 T. Isothermal magnetization curves were recorded at various temperatures in magnetic fields ranging from −1.5 to 1.5 T. The high-pressure electronic transport properties of $La_{1-x}Y_xO$ were measured through four-probe electrical conductivity methods in diamond anvil cells (DACs) made of CuBe alloy. The diamond culet is 300 μm in diameter. Au wires with diameter of 18 μm were used as electrodes. A T301 stainless steel gasket was compressed from thickness of 250 to 40 μm, and a hole of 150 μm in diameter was drilled by laser. Cubic BN as an insulating layer was pressed into this hole. A small central hole with diameter of 100 μm was further drilled to serve as the sample chamber, where NaCl fine powder serves as a pressure transmitting medium and a piece of compressed $La_{1-x}Y_xO$ powder sample with dimensions of 90 × 90 × 20 μm^3 was loaded. A ruby ball was loaded simultaneously as a pressure indicator. The assembled DACs were placed inside a cryogenicsystem with automatic temperature control.

DFT Calculations

First-principles calculations are performed by using density functional theory (DFT) as implemented in the Vienna ab initio simulation package (VASP)[24,25] with the projector augmented wave method[26] and the exchange-correlation functional within the generalized gradient approximation.[27] For the geometric structure relaxation, the total energy and the force on each atom are converged within 10^{-7} eV and less than 10^{-3} eV/Å, respectively. A plane-wave cutoff energy of 600 eV is adopted. The Brillouin zone (BZ) is sampled with a 11 × 11 × 11 k-point mesh for bulk LaO. The Fermi surface is obtained by interpolating the Hamiltonian on the basis of maximally localized Wannier functions using the Wannier90 package,[28,29] where the electronic structure around the Fermi level (E_F) is described by 15 Wannier functions (three p states for each O atom and five d and seven f states for the La atom).

Lattice dynamics and electron−phonon calculations are performed by using density functional perturbation theory as implemented in the QUANTUM ESPRESSO package,[30,31] with the norm-conserving pseudopotentials, an energy cutoff of 80 Ry, and a sampling of the electronic (vibrational) BZ by 12 × 12 × 12 (6 × 6 × 6) meshes. The electron−phonon matrix elements are calculated using a dense 24 × 24 × 24 k-point mesh. The superconducting critical temperature is evaluated through the Allen−Dynes modified McMillan formula[32] with a typical Coulomb pseudopotential μ^* = 0.13.[17]

3. RESULTS AND DISCUSSION

Crystal Structure

The as-made bulk LaO crystallizes in the characteristic NaCl-type structure ($Fm\bar{3}m$),[33] which is consistent with other reported rare earth monoxides (*RE*Os,[34−39] Figure 1a). Rietveld refinements of room-temperature SPXD data yielded the lattice parameter of a = 5.1451(2) Å, which is smaller than the previously reported dimensions in LaO thin films (5.351 Å), and consistent with reported one in bulk (5.144 Å). The ionic radius of La^{2+} is estimated to be 1.173 Å in our bulk phase, which is very comparable with the reported value of six-coordinate La^{2+} (1.25 Å).[40] Specifically, epitaxial LaO films on $YAlO_3$ substrates adopt a reduced lattice parameter (cube root of unit cell) of 5.202 Å, while those grown on $LaAlO_3$ and $LaSrAlO_4$ substrates show expanded lattice parameters of 5.245 and 5.298 Å, respectively, under tensile strain.[15] The significant variations in these lattice parameters mainly originate from the interfacial lattice mismatch between films and substrates, with their lattice mismatch degrees being 38.6, 91.2, and 93.1%, respectively. This effect will induce different degrees of lattice strain during the epitaxial growth process. Upon Y doping in $La_{1-x}Y_xO$, XRD peaks shift to higher diffraction angles with increasing Y content (x) up to 0.10 (Figure 1b), indicating a decrease in the lattice parameter a.[41] For x = 0.15, diffraction peaks corresponding to a secondary phase $LaYO_3$ appear. Refinements confirmed the decreasing trend in the primary phase, yielding lattice parameters a of 5.1451(2), 5.1398 (6), and 5.1294(4) Å for x = 0, 0.05, and 0.10, respectively (Supporting Information Figure S1). These findings suggest that the solubility limit of Y in LaO under the employed synthesis conditions is approximately x = 0.10 within the experiment error.

Magnetism

The superconducting properties of $La_{1-x}Y_xO$ (x = 0, 0.05, 0.10) were first investigated through magnetization measurements under ambient pressure. Figure 1c presents the temperature dependence of magnetization, $M(T)$, measured in ZFC and FC modes under an applied field of 30 Oe for x = 0, 0.05, and 0.10. All samples exhibit a distinct diamagnetic transition with an estimated superconducting shielding fraction approaching 100%, confirming bulk superconductivity. The bulk superconductivity is further evidenced by Specific heat (Figure S2). The onset transition temperatures (T_C(mag)), determined from the $M(T)$ curves, are approximately 5.58, 5.95, and 6.38 K for x = 0, 0.05, and 0.10, respectively. Note that La is a superconductor with T_C = 4.9 K, thus the possibility of superconductivity from La can be excluded. Magnetization versus magnetic field, $M(H)$, curves were measured for the parent LaO sample (Figure 1d), exhibiting typical type-II superconductivity.

Electrical Conductivity

To investigate the normal-state and superconducting characteristics, electrical resistivity measurements were performed on $La_{1-x}Y_xO$ (x = 0, 0.05, 0.10). As shown in Figure S3, the normal-state temperature dependence of resistivity, $\rho(T)$,

https://doi.org/10.1021/jacs.6c00519
J. Am. Chem. Soc. 2026, 148, 13309−13316

displays typical metallic behavior for all compositions. Figure 1e provides an enlarged view of the superconducting transition region under ZFC. These T_C are consistent with magnetization measurements. Notably, the T_C of our bulk LaO (6.05 K) is approximately 1 K higher than the previously reported value of ~5 K in LaO thin films. Figure S4 shows the $\rho(T)$ curves under various applied magnetic fields for representative samples. The criterion of 90% ρ_n (ρ_n, normal-state resistivity) is used to estimate upper critical field (H_{C2}). The temperature dependences of H_{C2} of x = 0, 0.05, and 0.10 are shown in Figure 1f. Using the Ginzburg–Landau (GL) formula, $H_{C2}(T) = H_{C2}(0) \times (T_{C0}^2 - T^2)/(T_{C0}^2 + T)$, where T_{C0} is the T_C under zero magnetic field, and $H_{C2}(0)$ is H_{C2} at zero temperature, the largest $H_{C2}(0)$ (≈3.85 T) is obtained for x = 0.10. The coherence length at zero temperature ($\xi(0)$) can be estimated using $H_{C2}(0) = \Phi_0/2\pi\xi(0)^2$, where $\Phi_0 = h/2e$ is the magnetic flux quantum. We obtain $\xi(0)$ = 93 Å for Y = 0.10, and it is comparable with nickelates.[42]

Chemical and Physical Pressure-Enhanced Superconductivity

Substituting La with smaller Y ions induces chemical pressure via lattice contraction.[43,44] Unlike the positive dependence of T_C on the cell expansion in LaO film, the chemical pressure enhances T_C in bulk LaO upon cell contraction. Hall effect measurements performed at 10 K elucidate the normal-state carrier concentration of LaO and $La_{0.9}Y_{0.1}O$. As shown in Figure S5, the calculated electron carrier concentration (n_e) increases from 2.5 × 10^{22} cm^{-3} in LaO to 3.3 × 10^{22} cm^{-3} in $La_{0.9}Y_{0.1}O$, indicating that Y doping effectively enhances the electron density in this system. It is consistent with the result that the Y-doped sample has the higher conductivity. The close correlation between carrier concentration and T_C has been studied extensively.[45] Here the positive correlation indicates the possibility of further optimizing T_C with extra carrier concentration.

In situ XRD and electrical resistance measurements were performed on LaO up to 53 GPa as shown in Figure 2a. No phase transition was observed during the compression as shown in Figure S6. The resulting pressure dependence of the superconducting transition temperature, $T_C(P)$, reveals several distinct regimes. Initially, T_C rises sharply from its ambient pressure value of ~6 to 11.8 K by 2.5 GPa. This rapid enhancement is followed by a more gradual increase, with T_C reaching a maximum of 12.7 K around 20.1 GPa. Between approximately 20.1 and 25.3 GPa, T_C exhibits a plateau before gradually declining upon further pressure increase beyond 25.3 GPa. This evolution traces a distinct dome-shaped $T_C(P)$ phase diagram (Figure 2b), suggesting the influence of competing pressure-induced effects on superconductivity.[46] Such dome-shaped pressure-dependence reminiscences pressure effects on numerous unconventional superconductors, including iron-based superconductors with multiorbital multiband nature. For LaO, the possible band splitting, which is indicated by our DFT calculations in following section, will be clarified experimentally in a separated work in the future.

To clarify the apparent discrepancy between bulk and thin-film LaO, it is instructive to compare their lattice tuning mechanisms. In epitaxial LaO films, superconductivity is stabilized only under tensile strain imposed by the substrate, which introduces anisotropic lattice distortion and reduces the cubic symmetry. In contrast, bulk LaO allows isotropic lattice tuning via chemical substitution and hydrostatic pressure while

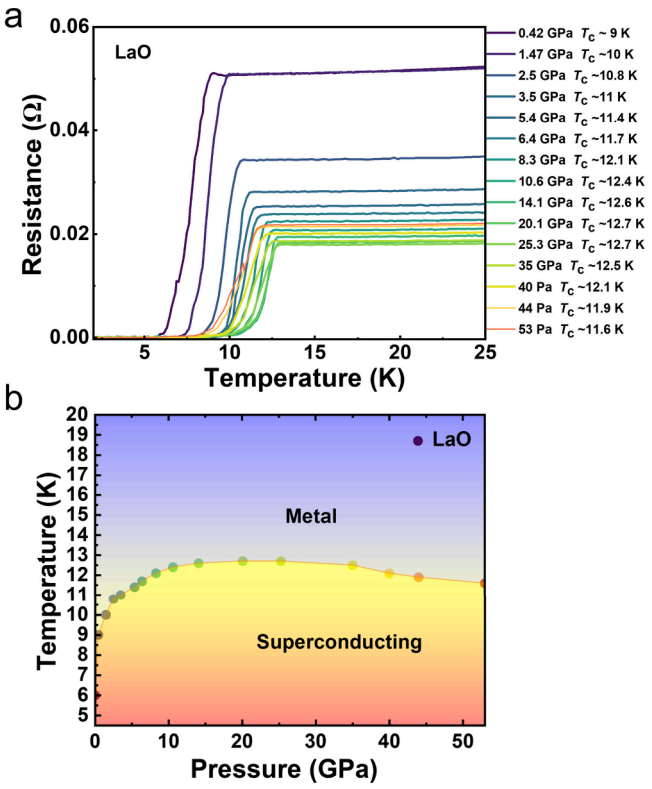

Figure 2. (a) Temperature dependence of the resistance of LaO at various pressures. (b) Pressure dependence of the superconducting transition temperature in LaO. (The sample exhibits superconductivity in the orange-yellow region and metallic properties in the blue-white region.)

preserving the rock-salt symmetry, and both routes consistently enhance T_C. Notably, the enhancement of T_C under compression in bulk LaO is opposite to the strain dependence reported in thin films, indicating that strain and pressure act through distinct microscopic mechanisms. While anisotropic strain mainly modifies crystal-field anisotropy and band degeneracy, isotropic compression enhances La 5*d*–O 2*p* hybridization and interorbital hopping, promoting superconductivity in a three-dimensional electronic environment. This contrast highlights bulk LaO as a platform to access the intrinsic superconducting state free from interfacial and substrate-clamping effects.

Electronic Structure Evolution and Superconducting Mechanism under Compressive Strain

To understand the superconducting mechanism of bulk LaO, we calculated its electronic properties and superconducting critical temperature (T_C) under isotropic compressive strain (uniform compression in *a*, *b*, *c* axes), focusing on orbital hybridization, crystal field splitting, and Fermi surface topology. As shown in Figure 3, the calculated band structures and DOS of bulk LaO under unstrained and 8% compressive strain reveal a metallic character, with one band crossing E_F. The electronic states near E_F are mainly derived from La 5*d* orbitals, with minor contributions from La 4*f* orbitals, while O 2*p* orbitals contribute negligibly. Under 8% compressive strain, the DOS at E_F decreases by approximately 17% (from 0.98 to 0.81 states/(eV·f.u.)), suggesting that compression reduces the number of available conducting states.

The strain-dependent evolution of the band structures and DOS (Figures S7 and S8) further confirms that compressive

https://doi.org/10.1021/jacs.6c00519
J. Am. Chem. Soc. 2026, 148, 13309–13316

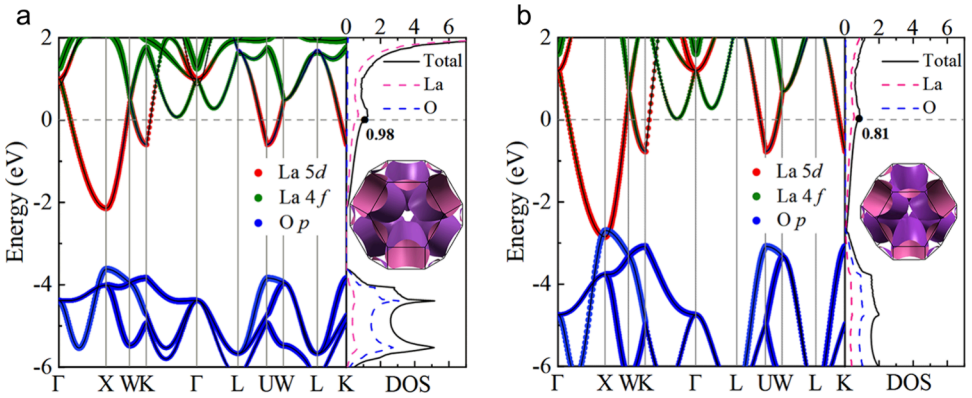

Figure 3. Electronic band structures and density of states of bulk LaO in (a) unstrained and (b) 8% isotropic compressive strain, with orbital characteristics superimposed on the band structure. The gray dashed line represents the Fermi level. Insets show the corresponding Fermi surface topologies.

Table 1. Tight-Binding Parameters of Bulk LaO under Unstrained and 8% Compressive Strain[a]

Strain	i	j	$t^{d_{x^2-y^2}}_{[i,j]}$	$t^{d_{z^2}}_{[i,j]}$	$t^{d_{xz}}_{[i,j]}$	$t^{d_{yz}}_{[i,j]}$	$t^{d_{xy}}_{[i,j]}$
0	0	0	4.4151	4.3813	2.5289	2.5404	2.5287
	1	0	−0.2099	0.0414	−0.1133	0.2514	−0.9288
−8	0	0	6.4138	6.2782	3.6365	3.6453	3.6463
	1	0	−0.2011	−0.0891	−0.2388	0.3179	−1.2815
Strain	i	j	$t^{d_{x^2-y^2}-d_{P_x}}_{[i,j]}$	$t^{d_{z^2}-d_{P_x}}_{[i,j]}$	$t^{d_{xz}-d_{P_z}}_{[i,j]}$	$t^{d_{yz}-d_{P_y}}_{[i,j]}$	$t^{d_{xy}-d_{P_y}}_{[i,j]}$
0	1	0	−1.497205	0.8303	0.7068	−0.0184	0.7037
−8	1	0	−2.210143	1.3439	0.7969	0.0004	0.7924

[a] $t^{d_m}_{[i,j]}$ and $t^{d_m-d_n}_{[i,j]}$ denote intra- and interorbital hopping, respectively, between sites [0,0] and [i,j]. All values are in eV.

strain strongly regulates the electronic structure. With increasing strain, the DOS near E_F continuously decreases. According to conventional BCS theory, such a reduction is unfavorable for Cooper pair formation, and T_C is expected to decrease accordingly. Indeed, the calculated T_C decreases with strain (Figure S9), and this trend is also consistent with the theoretical T_C calculation trend reported by Sun et al.10 However, experimental measurements under hydrostatic pressure show the opposite trend. It is hard to be explained by the phonon-mediated BCS mechanism, but rather likely originates from an unconventional pairing mechanism. Similarly, previous first-principles studies on compressed lanthanum-based compound LaBi also revealed that, the electron−phonon coupling mechanism based on weak BCS theory fails to account for the experimentally observed superconductivity (calculated T_C is close to 0 K, while the experimental T_C reaches up to ∼8 K), which also implies the existence of alternative superconducting mechanisms.[11]

Compared to the unstrained state (Figure 3a), the La 5d orbitals under 8% compressive strain (Figure 3b) exhibit a notable increase in bandwidth, implying enhanced dispersion and spatial delocalization. Specifically, the bottom of the La 5d orbitals at high-symmetry points (such as X) shifts downward, while the overall band moves upward relative to E_F. Meanwhile, the top of the O 2p orbitals shifts upward and shows increased dispersion, indicating a significant enhancement of La 5d−O 2p orbital hybridization. This dual modulation of the band edges—downshift of La 5d and upshift of O 2p—is attributed to the synergistic effects of enhanced crystal-field splitting and strengthened orbital hybridization induced by compressive strain.

As illustrated in the insets of Figure 3, the Fermi surface of bulk LaO displays a characteristic 3D topology, defined by multiple closed electron-like pockets symmetrically distributed around the Brillouin zone center. This structure signifies strong 3D dispersions and substantial spatial overlap between La 5d and O 2p orbitals, aligning with the enhanced hybridization observed in the band structure. The multipocket nature implies the coexistence of various Fermi scattering channels, offering favorable conditions for the multiband interactions required for unconventional superconductivity. When subjected to an 8% compressive strain, these electron pockets shrink and deform, concurrently enhancing the 3D connectivity between adjacent pockets. This strain-induced reconstruction reflects increased orbital overlap and electronic itinerancy, consistent with the enlarged hopping parameters and broadened bandwidths presented in Table 1. Notably, the existence of multiple nesting vectors in the 3D Fermi surface may amplify collective excitations, such as spin or orbital fluctuations, which are widely regarded as essential mediators of unconventional pairing. This suggests that La-based compounds, particularly those centered on 5d orbitals, may host a new class of systems driven by unconventional pairing mechanisms.

As summarized in Table 1, the tight-binding parameters quantitatively capture the strain-induced splitting of La 5d orbitals, revealing enhanced crystal-field effects in the octahedral environment (Figure S9). Moreover, both intra- and interatomic hopping parameters increase significantly—e.g., $t^{d_{xy}}_{[1,0]}$ from −0.9288 to −1.2815 eV and $t^{d_{x^2-y^2}-d_{P_x}}_{[1,0]}$ from −1.4972 to −2.2101 eV—indicating strengthened electron itinerancy and orbital fluctuations. Consequently, compressive

https://doi.org/10.1021/jacs.6c00519
J. Am. Chem. Soc. 2026, 148, 13309−13316

strain not only enhances electronic kinetic energy and orbital mixing, but may also promote the formation of an unconventional 3D superconducting pairing state through enhanced spin/orbital fluctuation mechanisms. In summary, bulk LaO exhibits unique electronic structure modulation under compressive strain, suggesting that it may be an unconventional 3D superconductor. This finding provides new insights into its superconducting mechanism and warrants further investigation.

The introduction of interfacial strain has been proven to be an effective way to achieve superconductivity at ambient pressure in state-of-the-art epitaxial thin-films, and thus to chemically realize and intercept the metastable superconductive state observed in bulk under physical pressure,[44] as exemplified in nickelate superconductors.[4,18,47,48−51] In our bulk LaO, the substitution of smaller Y^{2+} for larger La^{2+} leads to volumetric contraction of the unit cell and enhancement of the T_C from 6.05 to 6.9 K at 10% Y-doping. Meanwhile, the pressing of bulk LaO similarly squeezes the lattice and achieves the T_C as high as 12.7 K around 20 GPa. This maximum T_C is more than doubled than those in epitaxial films,[15,16] and even higher than the predicted record T_C of 11.11 K to date.[17] These findings suggest that smaller unit cell favors the superconductivity in bulk LaO, which is, however, in contradiction with the discoveries in thin films, where larger volume upon tensile stress favors higher T_C in films.[15,16]

Our experimental results are also inconsistent with DFT calculation based on phono-mediated Cooper paring, implying unconventional nature of LaO superconductivity. Future theoretical calculations, and/or in situ pressure- and temperature-dependent characterizations, will help to understand the rule for enhancing superconductivity in LaO and related systems with exotic electronic structure in rare-earth families.[52−55]

4. CONCLUSION

We have definitively resolved the long-standing ambiguity regarding the ground state of lanthanum monoxide. Contrary to early reports of metallic behavior, our high-pressure synthesis reveals that stoichiometric bulk LaO is an intrinsic type-II superconductor with T_C of ∼6 K. This value serves as a baseline that can be dramatically tuned: by applying "lattice compression"-either chemically via Y-substitution or physically via hydrostatic pressure-we achieved a continuous enhancement of T_C, culminating in a maximum of 12.7 K at 20 GPa. This is the highest transition temperature recorded in the lanthanum monochalcogenide family to date.

The most striking feature of our findings is the anomalous response of superconductivity to lattice compression, which provides a "smoking gun" evidence against a conventional phonon-mediated mechanism. In epitaxial thin films, superconductivity was believed to rely on lattice expansion (tensile strain). In stark contrast, we find that compression drives the T_C enhancement in the bulk. Crucially, our DFT calculations show that isotropic compression significantly suppresses the DOS at the E_F. According to the standard BCS formalism (specifically, the McMillan formula), such a reduction in phase space for pairing should inevitably suppress T_C. The experimental observation that T_C doubles while the DOS decreases fundamentally challenges the phonon-mediated scenario, strongly suggesting that the pairing glue in LaO is electronic in origin.

We propose that this unconventional superconductivity arises from the unique proximity of La 5*d* orbitals to the Fermi level. Unlike most La-based superconductors where La is trivalent, the divalent La in LaO possesses active 5d electrons. Our electronic structure analysis reveals that compressive strain induces a "dual modulation": it simultaneously shifts the La 5d band edges downward and the O 2*p* bands upward. This energetic convergence enhances $p-d$ hybridization and delocalization, triggering a reconstruction of the Fermi surface. The resulting three-dimensional topology features multiple electron-like pockets with substantial nesting vectors, creating ideal channels for pairing mediated by spin or orbital fluctuations.

In summary, bulk LaO represents a paradigm shift from "strain-stabilized" to "intrinsic unconventional" superconductivity. The pressure-induced enhancement of T_C—uncoupled from the density of states—mirrors the behavior of high-T_C cuprates and iron-based superconductors, yet it occurs in a remarkably simple rock-salt structure driven by 5*d* electrons. This establishes LaO not merely as a new superconductor, but as a minimalist platform for dissecting the interplay between 5*d*-orbital correlations and unconventional pairing, offering a fresh perspective for designing rare-earth-based quantum materials.

■ ASSOCIATED CONTENT

Supporting Information

The Supporting Information is available free of charge at https://pubs.acs.org/doi/10.1021/jacs.6c00519.

Specific heat measurements, doped cell evolution, electrical resistance under ambient pressure and applied magnetic fields, Hall resistance, high-pressure XRD, and supplementary theoretical calculation diagrams (PDF)

■ AUTHOR INFORMATION

Corresponding Authors

Dao-Xin Yao − *State Key Laboratory of Optoelectronic Materials and Technologies, Guangdong Provincial Key Laboratory of Magnetoelectric Physics and Devices, School of Physics, Sun Yat-Sen University, Guangzhou 510275, P. R. China*; Email: yaodaox@mail.sysu.edu.cn

Zheng Deng − *Beijing National Laboratory for Condensed Matter Physics, Institute of Physics, Chinese Academy of Sciences, Beijing 100190, P. R. China*; Email: dengzheng@iphy.ac.cn

Yifeng Han − *School of Chemistry and Chemical Engineering, Hainan University, Haikou 570228, P. R. China*; orcid.org/0000-0002-7518-978X; Email: Yifenghan@hainanu.edu.cn

Man-Rong Li − *School of Chemistry and Chemical Engineering, Hainan University, Haikou 570228, P. R. China*; orcid.org/0000-0001-8424-9134; Email: limanrong@hainanu.edu.cn

Authors

Zhifan Wang − *School of Chemistry and Chemical Engineering, Hainan University, Haikou 570228, P. R. China*

Jingkai Bi − *Institute of Quantum Materials and Physics, Henan Academy of Sciences, Zhengzhou 450046, P. R. China*

Jiayuan Zhang − *State Key Laboratory of Optoelectronic Materials and Technologies, Guangdong Provincial Key Laboratory of Magnetoelectric Physics and Devices, School of*

Physics, Sun Yat-Sen University, Guangzhou 510275, P. R. China

Wenmin Li − *Institute of Quantum Materials and Physics, Henan Academy of Sciences, Zhengzhou 450046, P. R. China*

Yuxuan Liu − *Key Laboratory of Bioinorganic and Synthetic Chemistry of Ministry of Education, School of Chemistry, Sun Yat-sen University, Guangzhou 510006, P. R. China*

Changqing Jin − *Beijing National Laboratory for Condensed Matter Physics, Institute of Physics, Chinese Academy of Sciences, Beijing 100190, P. R. China*

Complete contact information is available at: https://pubs.acs.org/10.1021/jacs.6c00519

Author Contributions

#Z.W., J.B., and J.Z. contributed equally to this work.

Notes

The authors declare no competing financial interest.

■ ACKNOWLEDGMENTS

This research was supported by the National Natural Science Foundation of China (22090041, 22575071, 12404007, 12494591, 92165204, 92565303, and 22531001), the Guangdong Basic and Applied Basic Research Foundation (Grant No. 2022B1515120014), the Guangdong Provincial Quantum Science Strategic Initiative (GDZX2401010), the CAS Project for Young Scientists in Basic Research (No. YSBR-030), MOST of China (No. 2022YFA1403900), the High-level Talent Research Start-up Program Funding of Henan Academy of Sciences (241827046, 242027151, and 241827022), the Fundamental Research Fund of Henan Academy of Sciences (240627005), Research Center for Magnetoelectric Physics of Guang dong Province (2024B0303390001), and Beijing National Laboratory for Condensed Matter Physics (2023BNLCMPKF006). The synchrotron radiation experiments were performed at BL44B2 of SPring-8 with the approval of the Japan Synchrotron Radiation Research Institute (JASRI) (Proposal No. 2025A1497), and the authors are grateful for the help of the BL14B beamline of SSRF. We thank Prof. Shou-Shu Gong at Great Bay University for his helpful discussions.

■ REFERENCES

(1) Chu, C.; Hor, P.; Meng, R.; Gao, L.; Huang, Z.; Wang, Y. Evidence for superconductivity above 40 K in the La-Ba-Cu-O compound system. *Phys. Rev. Lett.* **1987**, *58* (4), 405−407.

(2) Segre, C.; Dabrowski, B.; Hinks, D.; Zhang, K.; Jorgensen, J.; Beno, M.; Schuller, I. Oxygen ordering and superconductivity in $La(Ba_{2-x}La_x)Cu_3O_{7+\delta}$. *Nature.* **1987**, *329* (6136), 227−229.

(3) Chen, X.; Zhang, J.; Thind, A. S.; Sharma, S.; Labollita, H.; Peterson, G.; Zheng, H.; Phelan, D. P.; Botana, A. S.; Klie, R. F.; et al. Polymorphism in the ruddlesden-popper nickelate $La_3Ni_2O_7$: Discovery of a hidden phase with distinctive layer stacking. *J. Am. Chem. Soc.* **2024**, *146* (6), 3640−3645.

(4) Wang, L.; Li, Y.; Xie, S. Y.; Liu, F.; Sun, H.; Huang, C.; Gao, Y.; Nakagawa, T.; Fu, B.; Dong, B.; et al. Structure responsible for the superconducting state in $La_3Ni_2O_7$ at high-pressure and low-temperature conditions. *J. Am. Chem. Soc.* **2024**, *146* (11), 7506−7514.

(5) Kakoi, M.; Oi, T.; Ohshita, Y.; Yashima, M.; Kuroki, K.; Kato, T.; Takahashi, H.; Ishiwata, S.; Adachi, Y.; Hatada, N.; et al. Multiband metallic ground state in multilayered nickelates $La_3Ni_2O_7$ and $La_4Ni_3O_{10}$ probed by La-NMR at ambient pressure. *J. Phys. Soc. Jpn.* **2024**, *93* (5), 053702.

(6) Kamihara, Y.; Watanabe, T.; Hirano, M.; Hosono, H. Iron-based layered superconductor $La[O_{1-x}F_x]FeAs$ (X = 0.05−0.12) with T_c = 26 K. *J. Am. Chem. Soc.* **2008**, *130* (11), 3296−3297.

(7) Skorupskii, G.; Trump, B. A.; Kasel, T. W.; Brown, C. M.; Hendon, C. H.; Dincă, M. Efficient and tunable one-dimensional charge transport in layered lanthanide metal-organic frameworks. *Nat. Chem.* **2020**, *12* (2), 131−136.

(8) Gong, Y.; Zhou, M.; Andrews, L. Spectroscopic and theoretical studies of transition metal oxides and dioxygen complexes. *Chem. Rev.* **2009**, *109* (12), 6765−6808.

(9) Ushakov, S. V.; Hong, Q. J.; Gilbert, D. A.; Navrotsky, A.; Walle, A. V. Thorium and rare earth monoxides and related phases. *Materials.* **2023**, *16* (4), 1350.

(10) Sankaralingam, S.; Jaya, S.; Pari, G.; Asokamani, R. The electronic structure and superconductivity of the lanthanum monochalcogenides LaX (X = S, Se, Te). *Phys. Status. Solidi. B* **1992**, *174* (2), 435−447.

(11) Han, Y.; Brugman, B. L.; Leinbach, L. J.; Guo, X.; Leinenweber, K.; Navrotsky, A. Thermochemical properties of high pressure neodymium monoxide. *Inorg. Chem.* **2024**, *63* (29), 13468−13473.

(12) Leger, J. M.; Yacoubi, N.; Loriers, J. Synthesis of rare earth monoxides. *J. Solid. State. Chem.* **1981**, *36* (3), 261−270.

(13) Carette, P. The ultraviolet emission spectrum of LaO. *J. Mol. Spectrosc.* **1990**, *140* (2), 269−279.

(14) Schamps, J.; Bencheikh, M.; Barthelat, J. C.; Field, R. W. The electronic structure of lao: Ligand field versus ab initio calculations. *J. Chem. Phys.* **1995**, *103* (18), 8004−8013.

(15) Kaminaga, K.; Oka, D.; Hasegawa, T.; Fukumura, T. Superconductivity of rock-salt structure LaO epitaxial thin film. *J. Am. Chem. Soc.* **2018**, *140* (22), 6754−6757.

(16) Gan, H.; Zhang, C.; Du, X. Z.; Jiang, P.; Niu, C. P.; Zheng, X. H.; Yin, Y. W.; Li, X. G. Insights into superconductivity of LaO from experiments and first-principles calculations. *Phys. Rev. B* **2021**, *104* (5), 054515.

(17) Sun, P. H.; Zhang, J. F.; Liu, K.; Han, Q.; Lu, Z. Y. First-principles study of the superconductivity in LaO. *Phys. Rev. B* **2021**, *104* (4), 045121.

(18) Wang, G.; Wang, N.; Lu, T.; Calder, S.; Yan, J.; Shi, L.; Hou, J.; Ma, L.; Zhang, L.; Sun, J.; et al. Chemical versus physical pressure effects on the structure transition of bilayer nickelates. *npj. Quantum. Mater.* **2025**, *10* (1), 1.

(19) Sun, R.; Jin, S.; Deng, J.; Hao, M.; Zhong, X.; Ma, Y.; Li, M.; Chen, X. Chemical pressure boost record-high superconductivity in van der waals materials $FeSe_{1-x}S_x$. *Adv. Funct. Mater.* **2021**, *31* (40), 2102917.

(20) Lavroff, R. H.; Munarriz, J.; Dickerson, C. E.; Munoz, F.; Alexandrova, A. N. Chemical bonding dictates drastic critical temperature difference in two seemingly identical superconductors. *PNAS.* **2024**, *121* (14), No. e2316101121.

(21) Zhai, H.; Munoz, F.; Alexandrova, A. N. Strain to alter the covalency and superconductivity in transition metal diborides. *J. Mater. Chem. C* **2019**, *7* (34), 10700−10707.

(22) Yan, L.; Qin, J.; Liang, B.; Wang, Q.; Geng, M. High-pressure induction and quantitative regulation of oxygen vacancy defects in lithium titanate. *Adv. Funct. Mater.* **2023**, *33* (34), 2301886.

(23) Coelho, A. A. Topas and topas-academic: An optimization program integrating computer algebra and crystallographic objects written in C^{+2}. *J. Appl. Crystallogr.* **2018**, *51* (1), 210−218.

(24) Kresse, G.; Furthmüller, J. Efficient iterative schemes for ab initio total-energy calculations using a plane-wave basis set. *Phys. Rev. B* **1996**, *54* (16), 11169−11186.

(25) Kresse, G.; Furthmüller, J. Efficiency of ab-initio total energy calculations for metals and semiconductors using a plane-wave basis set. *Comput. Mater. Sci.* **1996**, *6* (1), 15−50.

(26) Blöchl, P. E. Projector augmented-wave method. *Phys. Rev. B* **1994**, *50* (24), 17953−17979.

(27) Perdew, J. P.; Burke, K.; Ernzerhof, M. Generalized gradient approximation made simple. *Phys. Rev. Lett.* **1996**, *77* (18), 3865−3868.

(28) Marzari, N.; Mostofi, A. A.; Yates, J. R.; Souza, I.; Vanderbilt, D. Maximally localized wannier functions: Theory and applications. *Rev. Mod. Phys.* **2012**, *84* (4), 1419−1475.
(29) Pizzi, G.; Vitale, V.; Arita, R.; Blügel, S.; Freimuth, F.; Géranton, G.; Gibertini, M.; Gresch, D.; Johnson, C.; Koretsune, T.; et al. Wannier90 as a community code: New features and applications. *J. Phys.: Condens. Matter* **2020**, *32* (16), 165902.
(30) Giannozzi, P.; Baroni, S.; Bonini, N.; Calandra, M.; Car, R.; Cavazzoni, C.; Ceresoli, D.; Chiarotti, G. L.; Cococcioni, M.; Dabo, I.; et al. Quantum espresso: A modular and open-source software project for quantum simulations of materials. *J. Phys.: Condens. Matter* **2009**, *21* (39), 395502.
(31) Giannozzi, P.; Andreussi, O.; Brumme, T.; Bunau, O.; Buongiorno Nardelli, M.; Calandra, M.; Car, R.; Cavazzoni, C.; Ceresoli, D.; Cococcioni, M.; et al. Advanced capabilities for materials modelling with quantum espresso. *J. Phys.: Condens. Matter* **2017**, *29* (46), 465901.
(32) Allen, P. B.; Dynes, R. C. Transition temperature of strong-coupled superconductors reanalyzed. *Phys. Rev. B* **1975**, *12* (3), 905−922.
(33) Qian, J.; Shen, Z.; Wei, X.; Li, W. Z_2 nontrivial topology of rare-earth binary oxide superconductor LaO. *Phys. Rev. B* **2022**, *105* (2), L020508.
(34) Leger, J.; Aimonino, P.; Loriers, J.; Dordor, P.; Coqblin, B. Transport properties of SmO. *Phys. Lett. A* **1980**, *80* (4), 325−327.
(35) Leger, J.; Yacoubi, N.; Loriers, J. Synthesis of neodymium and samarium monoxides under high pressure. *Inorg. Chem.* **1980**, *19* (8), 2252−2254.
(36) Leger, J.; Yacoubi, N.; Loriers, J. Synthesis of rare earth monoxides. *J. Solid. State. Chem.* **1981**, *36* (3), 261−270.
(37) Saito, D.; Kaminaga, K.; Oka, D.; Fukumura, T. Itinerant ferromagnetism in rocksalt NdO epitaxial thin films. *Phys. Rev. Mater.* **2019**, *3* (6), 064407.
(38) Sakamoto, S.; Kaminaga, K.; Oka, D.; Yukawa, R.; Horio, M.; Yokoyama, Y.; Yamamoto, K.; Takubo, K.; Nonaka, Y.; Koshiishi, K. Hard and soft x-ray photoemission spectroscopy study of the new kondo system SmO thin film. *Phys. Rev. Mater.* **2020**, *4* (9), 095001.
(39) Uchida, Y.; Kaminaga, K.; Fukumura, T.; Hasegawa, T. Samarium monoxide epitaxial thin film as a possible heavy-fermion compound. *Phys. Rev. B* **2017**, *95* (12), 125111.
(40) Jia, Y. Q. Crystal radii and effective ionic radii of the rare earth ions. *J. Solid. State. Chem.* **1991**, *95* (1), 184−187.
(41) Cao, X.; Huang, A.; Liang, C.; Chen, H. C.; Han, T.; Lin, R.; Peng, Q.; Zhuang, Z.; Shen, R.; Chen, H. M.; et al. Engineering lattice disorder on a photocatalyst: Photochromic BiOBr nanosheets enhance activation of aromatic C-H bonds via water oxidation. *J. Am. Chem. Soc.* **2022**, *144* (8), 3386−3397.
(42) Zhang, Y.; Su, D.; Huang, Y.; Shan, Z.; Sun, H.; Huo, M.; Ye, K.; Zhang, J.; Yang, Z.; Xu, Y.; et al. High-temperature superconductivity with zero resistance and strange-metal behaviour in $La_3Ni_2O_{7-\delta}$. *Nat. Phys.* **2024**, *20* (8), 1269−1273.
(43) Zhou, X.; Zhao, M.-H.; Yao, S. M.; Dong, H.; Wang, Y.; Chen, B.; Xing, X.; Li, M. R. Calibration of local chemical pressure by optical probe. *Nati. Sci. Rev.* **2023**, *10* (9), nwad190.
(44) Zhao, W.; Zhang, J.; Sun, Z.; Xiao, G.; Zheng, H.; Li, K.; Li, M.-R.; Zou, B. Chemical synthesis driven by high pressure. *CCS. Chem.* **2025**, *7* (5), 1250−1271.
(45) Liu, P.; Lei, B.; Chen, X.; Wang, L.; Wang, X. Superior carrier tuning in ultrathin superconducting materials by electric-field gating. *Nat. Rev. Phys.* **2022**, *4* (5), 336−352.
(46) Stewart, G. Unconventional superconductivity. *Adv. Phys.* **2017**, *66* (2), 75−196.
(47) Zhou, G.; Lv, W.; Wang, H.; Nie, Z.; Chen, Y.; Li, Y.; Huang, H.; Chen, W. Q.; Sun, Y. J.; Xue, Q. K.; et al. Ambient-pressure superconductivity onset above 40 k in $(La,Pr)_3Ni_2O_7$ films. *Nature.* **2025**, *640* (8059), 641−646.
(48) Ko, E. K.; Yu, Y.; Liu, Y.; Bhatt, L.; Li, J.; Thampy, V.; Kuo, C. T.; Wang, B. Y.; Lee, Y.; Lee, K.; et al. Signatures of ambient pressure superconductivity in thin film $La_3Ni_2O_7$. *Nature.* **2025**, *638* (8052), 935−940.
(49) Huo, Z.; Luo, Z.; Zhang, P.; Yang, A.; Liu, Z.; Tao, X.; Zhang, Z.; Guo, S.; Jiang, Q.; Chen, W.; et al. Modulation of the octahedral structure and potential superconductivity of $La_3Ni_2O_7$ through strain engineering. *Sci. China. Phys. Mech.* **2025**, *68* (3), 237411.
(50) Rhodes, L. C.; Wahl, P. Structural routes to stabilize superconducting $La_3Ni_2O_7$ at ambient pressure. *Phys. Rev. Mater.* **2024**, *8* (4), 044801.
(51) Jiang, R.; Hou, J.; Fan, Z.; Lang, Z. J.; Ku, W. Pressure driven fractionalization of ionic spins results in cupratelike high-T_c superconductivity in $La_3Ni_2O_7$. *Phys. Rev. Lett.* **2024**, *132* (12), 126503.
(52) Eick, H. A.; Baenziger, N. C.; Eyring, L. Lower oxides of samarium and europium. The preparation and crystal structure of $SmO_{0.4-0.6}$, SmO and EuO. *J. Am. Chem. Soc.* **1956**, *78* (20), 5147−5149.
(53) Ellinger, F. H.; Zachariasen, W. H. The crystal structure of samarium metal and of samarium monoxide. *J. Am. Chem. Soc.* **1953**, *75* (22), 5650−5652.
(54) Murthy, N. S.; Narasimhamurthy, B. Integrated intensities of the green-yellow system of lanthanum monoxide bands. *Nature.* **1969**, *223* (5202), 181−182.
(55) Li, W. L.; Chen, T. T.; Chen, W. J.; Li, J.; Wang, L. S. Monovalent lanthanide(i) in borozene complexes. *Nat. Commun.* **2021**, *12* (1), 6467.

https://doi.org/10.1021/jacs.6c00519
J. Am. Chem. Soc. 2026, 148, 13309−13316